Perturbing human V1 degrades the fidelity of visual working memory

Mrugank Dake[1] and Clayton E. Curtis[1, 2]

1. Department of Psychology, New York University
2. Center for Neural Science, New York University

Correspondence: clayton.curtis@nyu.edu

Keywords: working memory, transcranial magnetic stimulation, electroencephalography, memory-guided saccade, sensory recruitment, saccade, visual cortex

Abstract

The main function of working memory is to extend the duration with which information remains available for use by a host of high-level cognitive systems [1]. Decades of electrophysiological studies provide compelling evidence that persistent neural activity in prefrontal cortex is a key mechanism for working memory [2]. Surprisingly, sophisticated human neuroimaging studies have convincingly demonstrated that the contents of working memory can be decoded from primary visual cortex (V1) [3,4]. The necessity of this mnemonic information remains unknown and contentious. Here, we provide causal evidence that transcranial magnetic stimulation to human V1 disrupted the fidelity of visual working memory. Magnetic stimulation during the retention interval of a visuospatial working memory task caused a systematic increase in memory errors. Errors increased only for targets that were remembered in the portion of the visual field disrupted by stimulation, and were invariant to when in the delay stimulation was applied. Moreover, concurrently measured electroencephalography confirmed that stimulation disrupted not only memory behavior, but a standard neurophysiological signature of working memory. These results change the question from whether V1 is necessary for working memory into what mechanisms does V1 use to support memory. Moreover, they point to models in which the mechanisms supporting working memory are distributed across brain regions, including sensory areas that here we show are critical for memory storage.

Main

Our ability to maintain information no longer present in the environment, referred to as working memory, acts as a building block supporting most higher forms of cognition [1]. Indeed, impaired working memory can cause a cascade of broad cognitive symptoms in psychiatric disease [5]. Based on pioneering studies, the prefrontal cortex is theorized to store information in working memory in recurrent networks whose neural activity forms a mnemonic bridge between perception and memory-guided behavior [6,7]. There are two major pillars of support for this theory from studies of macaques. One, activity in prefrontal cortical neurons persists during memory delays [8]. Two, lesions to the macaque prefrontal cortex impair working memory performance [9]. More recently, human neuroimaging studies demonstrate that working memory representations may be widely distributed in the brain beyond the prefrontal cortex [10,11], including evidence for persistent neural activity in many cortical [4] and even subcortical areas [12]. Similarly, lesions to human cortical areas, both within and outside of the prefrontal cortex, impact working memory performance [13,14].

The most surprising finding in working memory research, which has now been replicated numerous times, is that the multivariate patterns of neural activity in primary visual cortex, V1, can be used to decode the contents of visual working memory [3,15]. Moreover, patterns in V1 are often the best for decoding the contents of working memory. Therefore, activity in V1 may encode representations needed for storing visual features in working memory, an idea that has been termed the sensory recruitment model of working memory. However, healthy skepticism exists about the necessity of V1 for working memory, as both macaque neurophysiology and human neuroimaging are mixed as to whether the neural activity in V1 persists during retention intervals [16], a hallmark of working memory. Perhaps the information decoded from V1 is not necessary for working memory despite being present. Lesions cannot resolve whether V1 is necessary for working memory because lesions to V1 would simply prevent visual encoding.

To overcome this impasse, here we directly tested whether human V1 is necessary for working memory using transcranial magnetic stimulation (TMS) to perturb neural processing during retention intervals. We first used fMRI to identify and model the receptive field properties of V1 [17]. Then, we identified the portion of V1 accessible to target with TMS - the dorsal part of the retinotopic map that represents the contralateral lower quadrant of the visual field (Figure 1A). We modeled the electric field induced by TMS [18] to target V1 in each participant (Figure 1B). These models indicated that TMS induced a greater electrical field in the V1 hemisphere targeted (Figure 1C). Targeting dorsal V1 with TMS induced phosphenes whose spatial extents were drawn by participants and allowed us to identify the phosphene field and its mirrored location (Figure 1D). Phosphene fields aligned well with the biophysical models we used to estimate the electric fields induced by TMS.

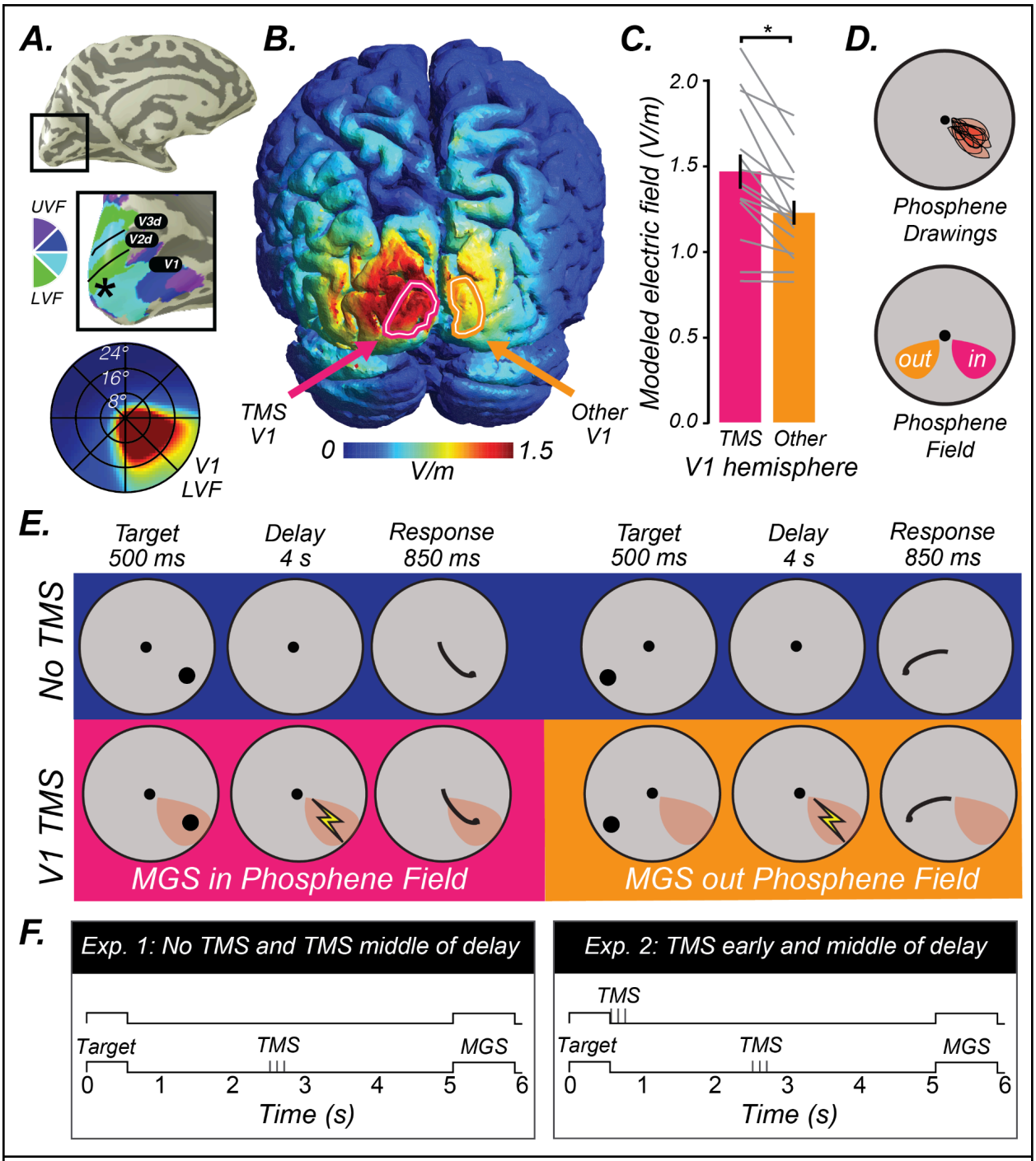

Figure 1. Working memory task conditions, trial types, and TMS procedures. A. In each participant, V1 was identified using population receptive field mapping [17]. Dorsal V1, which represents the contralateral lower visual field (LVF), was accessible to TMS stimulation (asterisk marks TMS target), while the upper visual field (UVF) is buried deeper and not accessible. The bottom radial plot depicts the group average visual field coverage of the dorsal V1 accessible to TMS, whose pRFs are localized to the lower visual field. **B.** The modeled electrical field induced by TMS targeting the retinotopically-defined left V1 (magenta encircled) for an example participant. V1 in the hemisphere opposite the one with TMS encircled by an orange line. See Supp Figure 1 for simulated electrical fields for all participants. Simulated electric field in Volts/meter (V/m). **C.** Based on the model [18], TMS induced a significantly larger electric field in the stimulated V1 compared to the V1 in the other hemisphere,

($t(14)=4.677$, $p=0.00035$). Thin gray lines are individual participants (N=15), bars are means (+/- SEM) across participants. **D.** In each participant, phosphene fields were defined as the portion of the visual field in which phosphenes were reliably evoked. TMS to dorsal V1 produced phosphenes in the contralateral lower visual field. Prior to memory experiments, participants drew with a mouse the extent of TMS-induced phosphenes (top). During the memory experiments, we placed visual targets in the phosphene field, and out of it(in the mirrored location) (bottom). **E.** Participants performed a memory-guided saccade (MGS) task, during which they maintained in working memory a target location. After a retention interval of 4 seconds, participants generated a memory-guided saccade. Feedback was then given, followed by an intertrial interval (2-3 s; not shown). We measured the accuracy of memory-guided saccades for targets in the phosphene field (experimental condition; magenta). Control conditions included no TMS (blue) and TMS to V1 when targets were in the hemifield opposite to the phosphene field (orange). **E.** Trial schematics for Experiment 1 and Experiment 2.

In Experiment 1, we measured the accuracy of memory-guided saccades for targets placed within the phosphene field (i.e., contralesional to TMS), and compared the performance to that when no TMS was applied and to that when the targets were placed in the hemifield opposite the phosphene field (i.e., ipsilesional to TMS) (Figure 1E/F). Remarkably, TMS applied to V1 during the middle of the delay caused larger memory errors, but only for targets within the phosphene field (Figure 2A). Specifically, memory errors were greater for targets inside the phosphene field compared to when no TMS was applied ($t(14)=2.431$, $p=0.013$), and compared to targets in the mirrored hemifield of the phosphene field ($t(14)=2.506$, $p=0.012$). No differences were found for errors for targets outside the phosphene field and no TMS ($t(14)=-0.678$, $p=0.745$) confirming the retinotopic specificity of the effect of TMS to V1 on working memory performance.

In Experiment 2, we aimed to both test the reproducibility of these results and how the timing of the stimulation impacts working memory performance. The same participants (n=15) returned and we again delivered TMS to V1 during the delay period of the memory-guided saccade task (Figure 1F). First, we perfectly replicated our findings from Experiment 1. TMS applied to V1 during the middle of the delay period caused greater memory errors for targets inside the phosphene field compared to targets in the mirrored hemifield ($t(14)=2.742$, $p=0.007$). Next, we asked how TMS applied during working memory maintenance compares to when applied during encoding (Figure 1F). TMS applied to V1 early in the delay at the offset of the visual target impaired memory accuracy for targets inside the phosphene field compared to targets outside it ($t(14)=3.303$, $p=0.003$). Although numerically larger, these errors caused by TMS at encoding were not statistically greater than those caused by TMS during maintenance ($t(14)=1.248$, $p=0.095$). TMS did not impact memory-guided saccade reaction times in either Experiment (Supp Figure 2; all p's>0.05). Together, these results demonstrate that perturbations to V1 are reliable, retinotopically specific, and are not limited to an epoch during which visual information undergoes consolidation into memory.

We used electroencephalography (EEG) in Experiment 1 to measure the impact that V1 TMS had on the characteristic asymmetry of alpha band topography over occipital cortex electrodes during working memory [19]. Without TMS, alpha power decreased in the hemisphere contralateral to the memory target early in the delay, which we quantified with an alpha lateralization index (Figure 2B, top). The lateralized alpha response persisted into the late portion of the delay, albeit lower in amplitude. On TMS trials, early in the delay the topography of alpha was indistinguishable from the no TMS trials before stimulation. Following TMS, the asymmetric

alpha response was reduced compared to no TMS (Figure 2B, bottom). Next, we subtracted the EEG time-frequency responses of the no TMS trials from the TMS trials among the occipital electrodes under the hemisphere in which stimulation was applied (see Methods). Once the TMS artifact resolved, we found significant reductions in alpha band power for about 500ms and beta band power for about 250ms (Figure 2C). Therefore, consistent with the increase in behavioral memory errors, TMS also disrupted a prominent EEG signature of working memory.

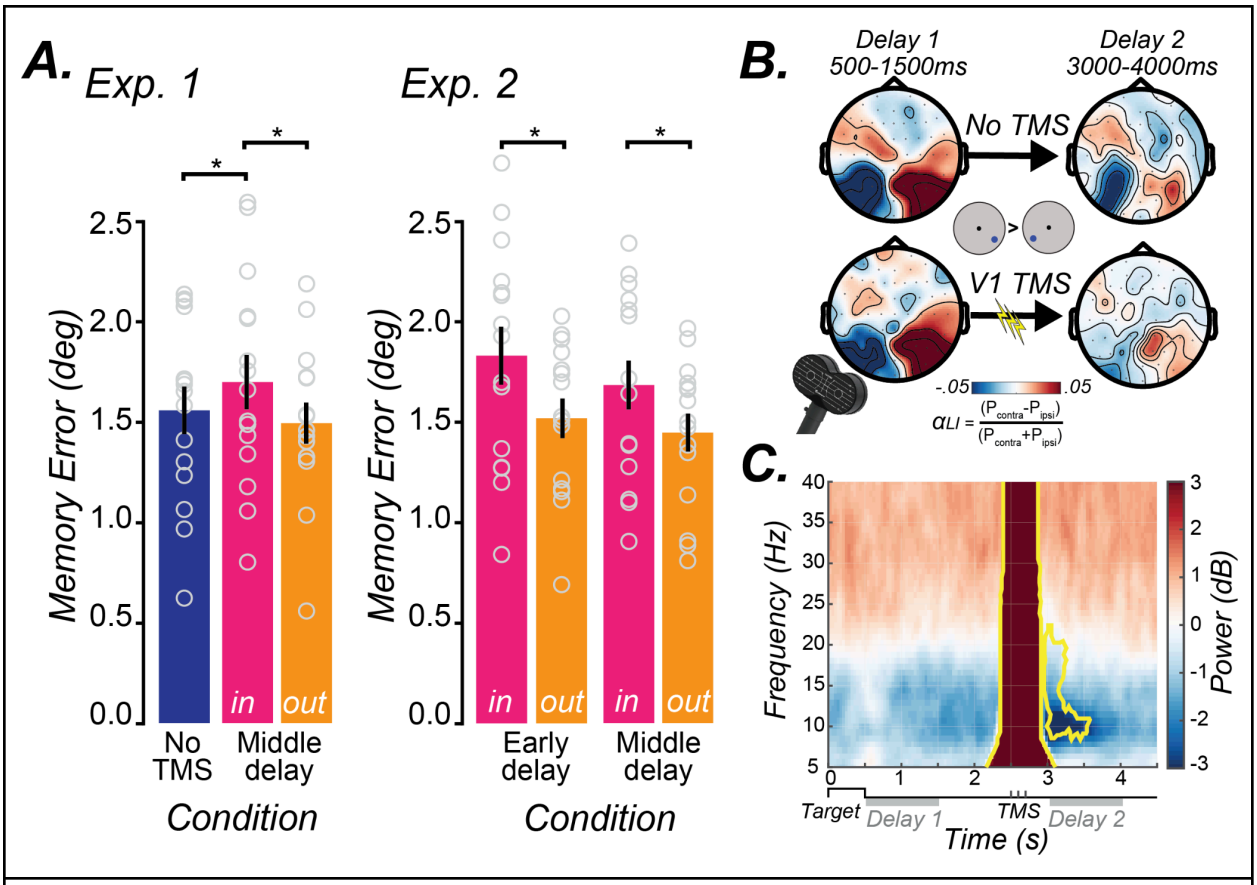

Figure 2. Effects of TMS to V1 on working memory A, In Experiment 1, TMS applied to V1 during the middle of the delay period caused an increase in memory errors for targets in the phosphene field (in), compared to when no TMS was applied and to memory for targets in the opposite hemifield (out). In Experiment 2, we replicated the results from Experiment 1 by again showing that TMS to V1 during the middle of the delay caused a specific worsening of memory for targets in the phosphene field. Moreover, we found similar effects when TMS to V1 was delivered as soon as the visual target was extinguished (early) and when it was applied later in the middle of the delay (middle). Bars depict means, with SEM error bars, and circles are individual participants. * denote $p<0.05$. **B.** EEG collected during Experiment 1 were used to compute an alpha lateralization index (αLI), sensitive to the topography of alpha power in electrodes over occipital cortex related to the location of working memory targets. Without TMS, alpha topography tracked the remembered targets evidenced by a decrease in alpha power contralateral to the target (Delay 1). This pattern persisted late into the delay period (Delay 2). Following TMS applied to V1 during the middle of the memory delay (2000 ms), note how the strength of the lateralized alpha decreased (Delay 2). **C**. EEG time-frequency responses during the working memory delay depicting the frequency of power changes caused by TMS to V1. Following the TMS evoked artifact (large red broadband increase), power significantly decreased in alpha and beta. Yellow outlines of significant clusters of power differences between no TMS minus TMS ($p<0.05$). The gray lines along the timeline denote the Delay 1 and Delay 2 epochs in B.

In summary, TMS to human V1 caused a deficit in working memory that was spatially restricted to the portion of the visual field perturbed by the electrical field induced by the TMS pulse. While previous studies testing how visual information is consolidated into working memory report that TMS to occipital cortex during the early encoding phase of working memory disrupts memory performance [20–22], we find that TMS during the maintenance phase produced deficits just as robust as those during encoding. Thus, our findings provide direct causal evidence that V1 is necessary for working memory, beyond simply the visual encoding or consolidation of stimuli into memory. Our findings bolster human neuroimaging studies that consistently report that the visual properties of memoranda stored in working memory can be decoded from the patterns of activity in V1 during retention intervals [4,10]. Moreover, they align with a subset of the neurophysiological recordings from macaque V1 demonstrating stimulus selective activity during working memory delays [23–25]. They provide a key piece of evidence that had been missing, but needed to directly test the sensory recruitment hypothesis of working memory. Indeed, we demonstrate that the neural mechanisms housed in V1 are necessary to maintain accurate working memory representations. Therefore, the question is no longer if visual cortex is necessary for working memory, but now it is by what mechanisms does it contribute to working memory?

Methods

Participants

Twenty-seven neurologically healthy humans (12 female, 15 male; mean age: 28, range: 21-55) were recruited to participate in multi-session TMS studies. All participants had normal to corrected normal vision and were screened for TMS eligibility and excluded from the study if they had any brain-related medical issues or were currently taking certain drugs (e.g. antidepressants, amphetamines, etc.). All participants provided written, informed consent and were compensated $50 for each session, regardless of whether it involved TMS (since the order of TMS was randomized across participants). Three participants found the procedures uncomfortable and withdrew. Five participants were withdrawn because we could not measure their gaze well enough (e.g., poor pupil lock, excessive blinking, lid closures, and dry/watery eyes). Since gaze was our main dependent variable, we could not study these participants. One participant was excluded because they did not follow instructions and made saccades only after the visual feedback was given, and thus not based on memory. Three participants were excluded because we could not reliably evoke phosphenes in the contralateral hemifield. The results, therefore, were based on fifteen participants (7 female, 8 male; mean age: 31, range: 21-55) who completed the full study. Two of the participants were authors and the rest were naive to the purpose of the study.

Rapid Serial Visual Presentation (RSVP) Task and Retinotopic Mapping

Anatomical and functional brain scans for pRF mapping were collected at New York University Center for Brain Imaging (CBI) using a 3T Siemens Prisma MRI scanner using a Siemens 64-channel head/neck radiofrequency coil. Volumes were acquired using a T2*-sensitive echo planar imaging pulse sequence (repetition time (TR), 1200 ms; echo time (TE), 36 ms; flip angle, 66°; 56 slices; 2 mm x 2mm x 2mm voxels). High-resolution T1-weighted images (0.8 mm x 0.8 mm x 0.8 mm voxels) were collected at the end of the session, with the same slice prescriptions as for the functional data, and used for registration, segmentation, and display. Multiple distortion scans (TR 6,000 ms; TE 63.4 ms; flip angle, 90°; 56 slices; 2 mm x 2 mm x 2 mm voxels) were collected during each scanning session.

To define visual field maps, each participant underwent retinotopic mapping in the MRI scanner, following previously established procedures [17]. Participants performed a RSVP task composed of sweeping bars of stimuli that swept across the screen in swift and discrete steps, moving in four possible directions: leftward to rightward, top to bottom, rightward to leftward, or bottom top. Each bar contained six images of colorful objects. At the start of each block, participants were shown the target object and were instructed to make a button press everytime the target object was present anywhere within the array while maintaining fixation. The participants received

online feedback with the fixation cross turning green indicating their response was accurate. The inter-stimulus interval was 400 ms and was titrated at the end of each sweep to match participants' accuracy to 70-80%. The data were monitored online for fixation breaks and blocks where participants broke fixation were eliminated from pRF model-fitting. Participants performed around 10 runs of the task, with 12 bar sweeps per run.

Resulting BOLD time series were fitted with a population receptive field (pRF) model with compressive spatial summation [26,27], and visual field maps, including V1, were drawn manually using afni and suma. Specifically, we visualized the polar angle and the eccentricity maps on the cortical surface, thresholded to include only voxels for which the pRF model explained more than 10% of the variance.

Transcranial Magnetic Stimulation (TMS)

The T1-weighted images of participants were used to reconstruct brain and skin surfaces to localize targets for TMS using a frameless stereotaxic neuronavigation system (Brainsight, Rogue Research Inc., CAN) combined with Polaris Spectra (Northern Digital, USA) infrared cameras that tracked markers positioned on the TMS coil and on the participant's head. TMS was applied using a MagVenture MagPro X100 stimulator with a MCF-B70 static cooled coil. TMS pulses were triggered and coupled with EEG using custom MATLAB and Python scripts (https://github.com/clayspacelab/EEG_TMS_triggers). We identified V1 in each participant from fMRI-based retinotopy (see *Retinotopic Mapping* above) and overlaid the target on the brain surface in Brainsight. We initially randomized whether the participant would receive TMS to the left or right V1. However, if we had difficulties evoking reliable phosphenes we would switch to the other hemisphere. Once we identified a putative target that evoked phosphenes, we then determined the phosphene threshold and mapped the spatial extent of the phosphene (see *Phosphene Mapping* next).

Phosphene Mapping

Participants were first screened for their ability to detect phosphenes in a dimly lit room by placing the TMS coil over retinotopically defined V1 and applying 7 pulses at 20 Hz. The coil was oriented with the handle away from the interhemispheric fissure to induce currents along the caudal-rostral axis. We made small changes to the position and angle of the TMS coil until we identified a trajectory that reliably induced phosphenes. If phosphenes were inconsistent or weak, we tried stimulating V1 in the other hemisphere. Next, we then measured the spatial extent and borders of phosphenes. Participants used a computer mouse to encircle the perceived phosphene on several trials until consistency was achieved, defined as at least three trials with overlapping phosphenes. For each participant, we defined their phosphene field (PF), which we derived from the overlapping area of the phosphene drawings. The PF was the area of visual space consistently

impacted by TMS to V1 at the given coil position. The area of the PF was determined by the following criteria. First, the centroid was calculated as the center of the overlapping area. Second, the angular extent spanned the full distance along an arc running through the centroid. Third, the radial extent was defined as a 2 degree band centered at the centroid. In the experiment, we placed memory targets inside the area of the defined PF (see *Memory-Guided Saccade Task* below). Once a reliable PF was identified, we estimated their phosphene threshold of TMS intensity. Starting at 30% of maximum stimulator output we delivered 7 pulses at 20 Hz and recorded if a phosphene was evoked. We increased the stimulation intensity by 10% until phosphenes were reliably evoked, then reduced stimulation intensity by 5% to find the threshold defined as reported phosphene in 5 out of 10 trials. In the main experiment, we used a stimulation intensity at 110% of that threshold, but only applied 3 pulses at 20 Hz.

Memory-Guided Saccade Task

Experiment 1: TMS during working memory maintenance. Middle Delay.

Participants performed a memory-guided saccade (MGS) task. Each block consisted of 40 trials and began with a fixation cross, followed by a target presented for 500ms inside the PF, or the mirrored hemifield of the PF, randomized across trials. Participants maintained in working memory the location of the target over a 4s retention interval while fixating a central circular fixation stimulus. When the fixation stimulus turned green, they made a saccade, guided by their memory alone, to the location of the target. After 850ms, the target reappeared in green serving as feedback. Experiments 1 and 2 were conducted over four days to minimize both fatigue and the number of TMS pulses participants experienced in a given day. On day 0, participants performed a 1 hour TMS session of phosphene thresholding, phosphene mapping (described above), and practice of MGS task. On days 1-3, participants performed 5 blocks (200 trials; 600 TMS pulses) of the MGS task during which their brain activity was recorded using EEG (see *Electroencephalography* below). On 2 of these 3 days, TMS was applied to V1 during the middle (at 2s) of the 4s long delay (what we refer to as *Middle Delay)*. On the other day, no TMS was applied. For each participant, we randomized the order of the days in which TMS was applied.

Experiment 2: TMS during working memory encoding. Early Delay.

Each participant returned on another day to complete two sessions of the MGS task, while TMS was applied to the V1 target area previously identified. EEG was not collected. The experiment was identical to that described in Experiment 1, with the only difference being that TMS was applied as soon as the target was offset (what we refer to as *Early Delay*) or in the middle of the delay (what we refer to as *Middle Delay*). The order of sessions was randomized across participants. Each session lasted for 40 minutes and participants performed 5-7 blocks of MGS

task (described above), followed by a mandatory 10-minute break before they performed the next session lasting 40 minutes.

Eye-tracking and Visual Display

Participants were seated in a dim-lit room with the head positioned on a chin-rest 56 cm away from a gamma-calibrated ViewPix monitor (120Hz refresh rate, 1920*1080 resolution) controlled by an Ubuntu video card. Stimuli were presented using MATLAB and Psychtoolbox [28]. An Eyelink 1000 Desktop Mount (SR Research) was used to record the right eye position at 1000 Hz. For all participants, a 9-point calibration was performed at the start of the session and repeated whenever the participant took a break by moving the head from the chin-rest. The data were then preprocessed using iEye (https://github.com/clayspacelab/iEye), an in-house gaze-analysis toolbox written in MATLAB. The preprocessing involved multiple steps. First, blinks were identified as pupil diameter lower than 1 percentile. Gaze data 100 ms before and after blinks were removed. Next, a Gaussian smoothing kernel was applied to gaze traces to get an estimation of velocity. This was used to detect saccades, which were defined as gaze transitions with velocities greater than 30 deg/s, having an amplitude greater than 0.25 degree, and a duration of at least 7.5 ms. The data were then corrected for any instrumental drift by demeaning the gaze traces during fixation and delay epochs. Lastly, we also performed calibration using the corrective saccades during the feedback for any instrumental or head-movement-related drift that might have occurred in a trial. Given eye-tracking was the sole-metric of behavior, these extra precautions ensured quality gaze data.

Electroencephalography (EEG)

We used a BrainProducts 64-channel actiChamp system with low-profile active electrodes for recording EEG activity. Data were sampled at 1000Hz, with the ground placed at the center of forehead above nasion and Cz was used as the online reference. EEG data were analyzed using Fieldtrip toolbox [29]. Any trials with errors in timing of the TMS pulse were detected (less than 2 out of 400 trials on average per session) and removed from analysis. Then, the data for each session were band-pass filtered between 0.5-50 Hz using a two-pass butterworth filter of filter order 4. The data were then screened for bad channels. Bad channels were identified as ones that exhibited more than 90 percentile of median variance amongst all channels, were flat (std < 0.01 μV) or were extremely noisy (std > 100 μV) [30]. The cleaned data were then offline re-referenced to the common average. Next, owing to long delays in our working memory task, the data were heavily contaminated with blink artifacts. Independent Component Analysis (ICA) was performed using the 'fastica' algorithm in Fieldtrip and components exhibiting muscle twitches, eye-movement artifacts and saccades were carefully examined and eliminated. Bad channels removed earlier were then interpolated using a weighted interpolation of neighboring electrodes. The data were then epoched and downsampled to 200Hz. The epoched data were then examined

for bad trials which were then eliminated (less than 0.5% on average). Additionally, time-frequency analysis (TFA) was conducted to investigate spectral dynamics. The analysis was performed using the wavelet method. The frequency range was set from 2 to 40 Hz, discretized into 53 linearly spaced frequency bins. The number of cycles for the wavelet analysis varied linearly with frequency, ranging from 4 to 15 cycles across the specified frequency range. Subsequently, the power values were converted to decibel (dB) scale. Alpha Lateralization Index (ALI) was computed as the ratio of power difference between the contralateral and ipsilateral activity for each trial from the occipito-parietal electrodes (O1, O2, PO3, PO4, PO7, PO8, P1, P2, P3, P4, P5, P6, P7, P8) to the total power across all occipito-parietal electrodes.

$ALI = (P_{contra} - P_{ipsi}) / (P_{contra} + P_{ipsi})$

where, P_{contra} was power in an electrode on trials where stimulus was present in contralateral hemifield, and P_{ipsi} was power in an electrode on trials where stimulus was present in ipsilateral hemifield.

Electrical field simulations

Simulation of Noninvasive Brain Stimulation (SimNIBS) [18] 4.0 was used to estimate the electric field induced in the brain based on anatomical scans and the target location chosen for each participant as described above. Using CHARM-based head-segmentation [31] and target locations, E-field estimates were computed for each individual brain taking into account conductivities of different tissue types. The model uses the coil specifications provided by MagVenture to estimate the magnetic field induced by the coil. For each participant, the exact placement of the TMS coil, including the rotational angle was input to the model. Our aim was to create biophysical models of the amplitude and extent of the electric field induced by TMS to V1 for each participant.

Statistical Analyses

We conducted paired t-tests using trial-level permutations with SciPy [32]. Specifically, we randomly shuffled the trial labels for TMS conditions (No TMS, Early TMS, or Middle TMS) and target location (inside PF or outside PF). For each permutation, we computed the group average for each condition, thereby generating a null distribution of t-statistics. The observed t-statistic was then compared against this null distribution to obtain the p-value.

For time-frequency EEG analyses, we employed a cluster-based permutation approach to perform paired t-tests at each time-frequency bin using *ft_freqstatistics* function in Fieldtrip. The primary alpha level was set to 0.05, while the cluster threshold was set at cluster-alpha of 0.1. Significance of the clusters was assessed using Monte Carlo method with 1000 random permutations.

Acknowledgments

We thank the staff of the Center for Brain Imaging (CBI) at New York University (NYU), and Yuyang Xu and Qingqing Yang for help with data collection. We are also grateful to Nathan Tardiff for comments on drafts on the manuscript. Funded by NIH R01 EY- 016407 and R01 EY-033925 to C.E.C.

Data Availability

All data used in this study is made publicly available at osf.XYZ. The published dataset contains preprocessed and de-identified behavioral data across both experiments, EEG data from each session of experiment 1, and the TMS-efield simulations.

Code Availability

Code used to trigger the TMS and EEG systems is available at https://github.com/clayspacelab/EEG_TMS_triggers. The toolbox iEye used to process eye-tracking data is available at https://github.com/clayspacelab/iEye. And the code used for experiment design and analysis of behavioral and EEG data as well as for creating TMS E-field simulations is available at https://github.com/mindemory/mgs_stimul.

References

1. Conway, A. R. A., Kane, M. J. & Engle, R. W. Working memory capacity and its relation to general intelligence. *Trends Cogn. Sci.* **7**, 547–552 (2003).
2. Riley, M. R. & Constantinidis, C. Role of Prefrontal Persistent Activity in Working Memory. *Front. Syst. Neurosci.* **9**, 181 (2015).
3. Harrison, S. A. & Tong, F. Decoding reveals the contents of visual working memory in early visual areas. *Nature* **458**, 632–635 (2009).
4. Curtis, C. E. & Sprague, T. C. Persistent Activity During Working Memory From Front to Back. *Front. Neural Circuits* **15**, 696060 (2021).
5. Goldman-Rakic, P. S. Working memory dysfunction in schizophrenia. *J. Neuropsychiatry Clin. Neurosci.* **6**, 348–357 (1994).
6. Goldman-Rakic, P. S. Cellular basis of working memory. *Neuron* **14**, 477–485 (1995).
7. Fuster, J. The prefrontal cortex—an update time is of the essence. *Neuron* **30**, 319–333 (2001).
8. Funahashi, S., Bruce, C. J. & Goldman-Rakic, P. S. Mnemonic coding of visual space in the monkey's dorsolateral prefrontal cortex. *J. Neurophysiol.* **61**, 331–349 (1989).
9. Funahashi, S., Bruce, C. J. & Goldman-Rakic, P. S. Dorsolateral prefrontal lesions and oculomotor delayed-response performance: evidence for mnemonic 'scotomas'. *J. Neurosci.* **13**, 1479–1497 (1993).
10. Christophel, T. B., Klink, P. C., Spitzer, B., Roelfsema, P. R. & Haynes, J.-D. The Distributed Nature of Working Memory. *Trends Cogn. Sci.* **21**, 111–124 (2017).
11. Sreenivasan, K. K. & D'Esposito, M. The what, where and how of delay activity. *Nat. Rev. Neurosci.* **20**, 466–481 (2019).
12. Rahmati, M., DeSimone, K., Curtis, C. E. & Sreenivasan, K. K. Spatially Specific Working Memory Activity in the Human Superior Colliculus. *J. Neurosci.* **40**, 9487–9495 (2020).
13. Mackey, W. E., Devinsky, O., Doyle, W. K., Meager, M. R. & Curtis, C. E. Human Dorsolateral Prefrontal Cortex Is Not Necessary for Spatial Working Memory. *J. Neurosci.* **36**, 2847–2856 (2016).
14. Mackey, W. E., Devinsky, O., Doyle, W. K., Golfinos, J. G. & Curtis, C. E. Human parietal cortex lesions impact the precision of spatial working memory. *J. Neurophysiol.* **116**, 1049–1054 (2016).
15. Serences, J. T., Ester, E. F., Vogel, E. K. & Awh, E. Stimulus-Specific Delay Activity in Human Primary Visual Cortex. *Psychological Science* vol. 20 207–214 Preprint at https://doi.org/10.1111/j.1467-9280.2009.02276.x (2009).
16. Leavitt, M. L., Mendoza-Halliday, D. & Martinez-Trujillo, J. C. Sustained Activity Encoding Working Memories: Not Fully Distributed. *Trends in Neurosciences* vol. 40 328–346 Preprint at https://doi.org/10.1016/j.tins.2017.04.004 (2017).
17. Mackey, W. E., Winawer, J. & Curtis, C. E. Visual field map clusters in human frontoparietal cortex. *Elife* **6**, (2017).
18. Thielscher, A., Antunes, A. & Saturnino, G. B. Field modeling for transcranial magnetic stimulation: A useful tool to understand the physiological effects of TMS? in *2015 37th Annual International Conference of the IEEE Engineering in Medicine and Biology Society (EMBC)* 222–225 (2015).
19. Medendorp, W. P. *et al.* Oscillatory activity in human parietal and occipital cortex shows hemispheric lateralization and memory effects in a delayed double-step saccade task. *Cereb. Cortex* **17**, 2364–2374 (2007).
20. van de Ven, V., Jacobs, C. & Sack, A. T. Topographic contribution of early visual cortex to short-term memory consolidation: a transcranial magnetic stimulation study. *J. Neurosci.* **32**, 4–11 (2012).
21. Cattaneo, Z., Vecchi, T., Pascual-Leone, A. & Silvanto, J. Contrasting early visual cortical activation states causally involved in visual imagery and short-term memory. *Eur. J. Neurosci.* **30**, 1393–1400 (2009).
22. van Lamsweerde, A. E. & Johnson, J. S. Assessing the Effect of Early Visual Cortex Transcranial Magnetic Stimulation on Working Memory Consolidation. *J. Cogn. Neurosci.* **29**, 1226–1238 (2017).

23. Fuster, J. M. & Jervey, J. P. Inferotemporal neurons distinguish and retain behaviorally relevant features of visual stimuli. *Science* **212**, 952–955 (1981).
24. van Kerkoerle, T., Self, M. W. & Roelfsema, P. R. Layer-specificity in the effects of attention and working memory on activity in primary visual cortex. *Nat. Commun.* **8**, 13804 (2017).
25. Supèr, H., Spekreijse, H. & Lamme, V. A. A neural correlate of working memory in the monkey primary visual cortex. *Science* **293**, 120–124 (2001).
26. Dumoulin, S. O. & Wandell, B. A. Population receptive field estimates in human visual cortex. *Neuroimage* **39**, 647–660 (2008).
27. Kay, K. N., Winawer, J., Mezer, A. & Wandell, B. A. Compressive spatial summation in human visual cortex. *J. Neurophysiol.* **110**, 481–494 (2013).
28. Brainard, D. H. The Psychophysics Toolbox. *Spat. Vis.* **10**, 433–436 (1997).
29. Oostenveld, R., Fries, P., Maris, E. & Schoffelen, J.-M. FieldTrip: Open source software for advanced analysis of MEG, EEG, and invasive electrophysiological data. *Comput. Intell. Neurosci.* **2011**, 156869 (2011).
30. Komosar, M., Fiedler, P. & Haueisen, J. Bad channel detection in EEG recordings. *Current Directions in Biomedical Engineering* **8**, 257–260 (2022).
31. Puonti, O. *et al.* Accurate and robust whole-head segmentation from magnetic resonance images for individualized head modeling. *Neuroimage* **219**, 117044 (2020).
32. Virtanen, P. *et al.* SciPy 1.0: fundamental algorithms for scientific computing in Python. *Nat. Methods* **17**, 261–272 (2020).

Supplementary Figures and Table

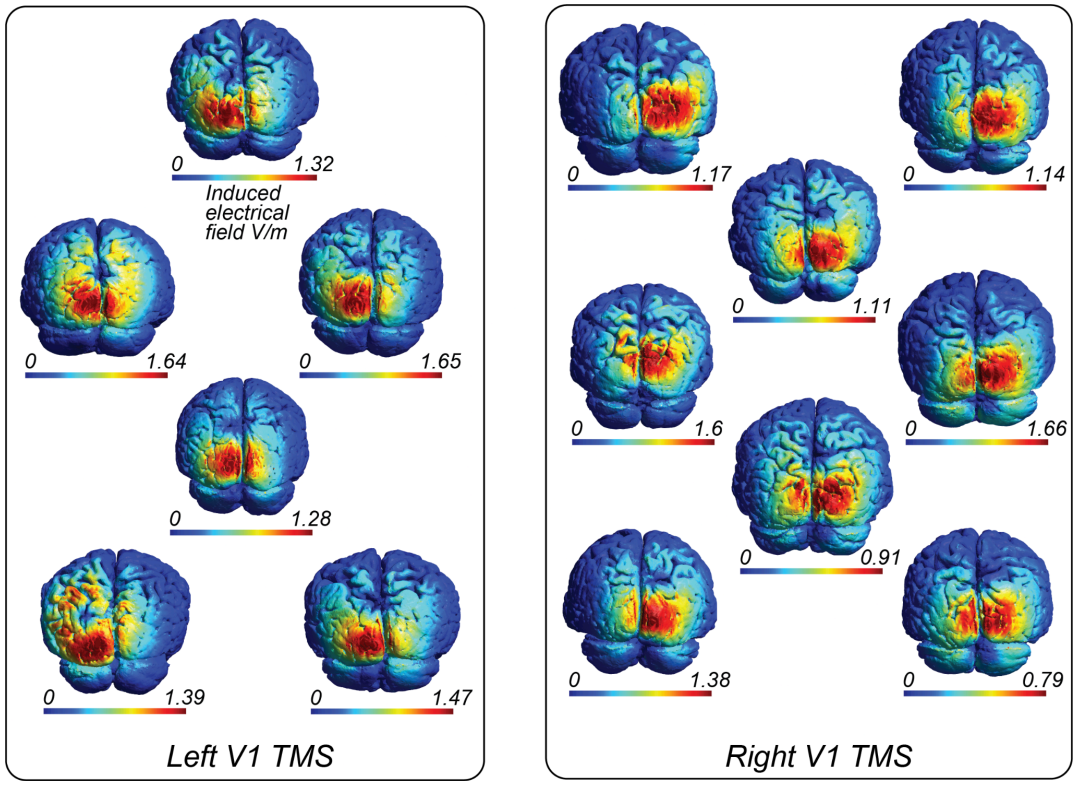

Supplementary Figure 1 — E-field simulations for individual participants: *Induced E-field (V/m) in individual brains as predicted by SimNIBS on native brains for a single pulse of TMS applied at the target location used for each participant. (Left) For participants with left V1 stimulated. (Right) For participants with right V1 stimulated.*

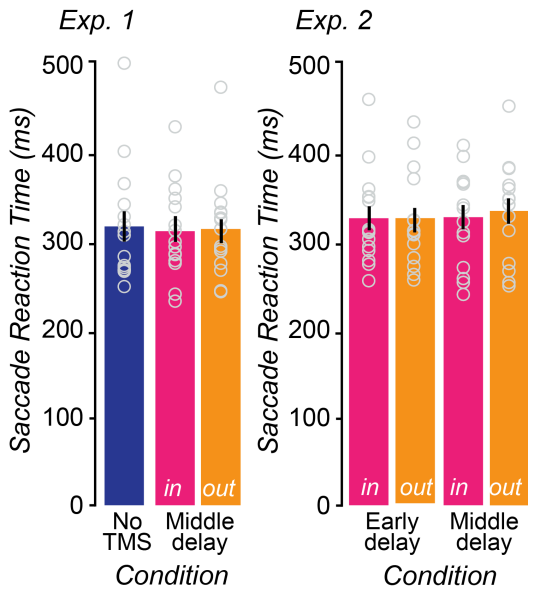

Supplementary Figure 2 — Effect of TMS on Reaction Time. *Saccade reaction times (sRT) (in ms) for different conditions. There was no impact of TMS on sRT either when TMS was applied during early or middle delay relative to No TMS ($p > 0.05$). Similarly, there was no difference in sRT for when targets were present inside or outside PF ($p > 0.05$) when TMS was applied during either the early or middle part of the delay.*

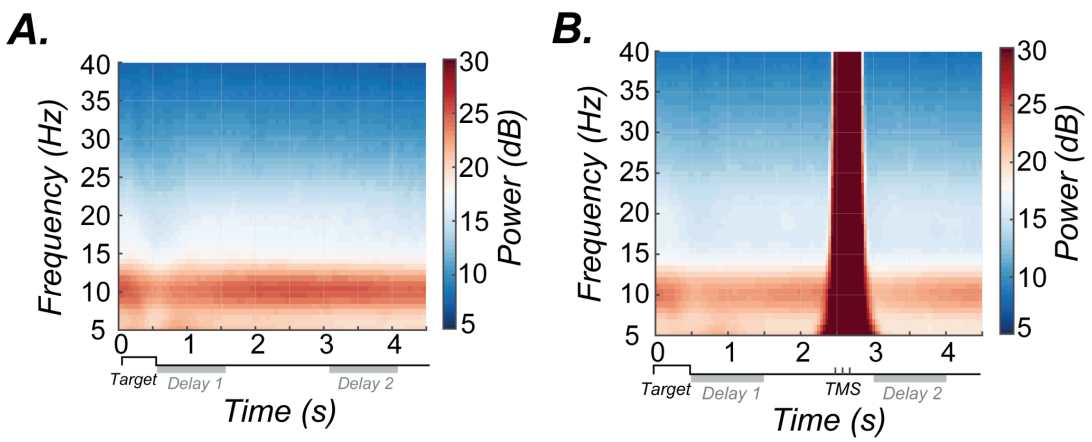

Supplementary Figure 3 — Time-Frequency Responses during Delay Period *A) No TMS, B) TMS, shows the time-freuqency responses averaged across participants for occipital electrodes under the TMS site.*

***Supplementary Table 1* — Participant demographics and stimulation parameters**

Participant	Sex	Race	Age (years)	Handedness	Hemisphere stimulated	Phosphene Threshold (% MSO)	Centroid of Phosphene [eccentricity (dva), polar angle (degrees)]
01	M	White	55	Right	Left	40	(14.2, 352.0)
02	F	Asian	25	Right	Right	42	(16.8, 192.9)
03	M	Asian	26	Right	Left	51	(11.6, 337.4)
04	F	Asian	27	Right	Right	62	(13.0, 193.8)
05	M	Asian	22	Left	Left	52	(14.3, 336.1)
06	F	Asian	29	Right	Right	42	(6.2, 186.8)
07	M	White	35	Right	Left	50	(7.48, 341.9)
08	M	Asian	26	Right	Right	40	(13.8, 208.6)
09	M	White	28	Left	Right	37	(16.0, 196.1)
10	M	Asian	26	Right	Left	44	(12.2, 334.4)
11	F	Asian	30	Right	Right	43	(11.5, 183.6)
12	M	Asian	30	Right	Right	48	(14.3, 200.1)
13	M	Asian	22	Right	Right	43	(16.2, 215.8)
14	F	Asian	32	Right	Left	35	(6.6, 345.7)
15	F	More than one	21	Right	Left	43	(12.8, 330.0)